Where do the counterions go? Tip-induced dissociation of self-assembled triazatriangulenium-based molecules on Au(111)

S. Snegir, Y. J Dappe, D. Sysoiev, O. Pluchery, T. Huhn, E. Scheer

Where are the counterions gone? Tip-induced dissociation of self-assembled triazatriangulenium–based molecules on Au(111)

S. Snegir[*,1], Y. J. Dappe[2], D. Sysoiev[3,4], O. Pluchery[5], T. Huhn[3], E. Scheer[1]

[1]Department of Physics, University of Konstanz, Universitätsstraße 10, 78464 Konstanz, Germany

[2]SPEC, CEA, CNRS, Université Paris-Saclay, CEA Saclay, 91191 Gif-sur-Yvette Cedex, France

[3]Department of Chemistry, University of Konstanz, Universitätsstraße 10, 78464 Konstanz, Germany

[4] Current address: Institute of Organic Chemistry and Biochemistry, Czech Academy of Sciences Flemingovo nam. 2, 16610 Prague (Czech Republic).

[5]Sorbonne Université, CNRS, Institut des NanoSciences de Paris (INSP), 4 place Jussieu, 75005 Paris, France.

* corresponding author

Corresponding Author

* sergii.snegir@uni-konstanz.de

ABSTRACT: Chemical coupling of functional molecules on top of so-called platform molecules allows the formation of functional self-assembled monolayers (SAMs). An often-used example of such a platform is triazatriangulenium (TATA), which features an extended aromatic core providing good electronic contact to the underlying metal surface. Here we present a study of SAM formation of the TATA platform on Au(111) employing scanning tunneling microscopy (STM) in ambient atmospheric conditions. In solution, the TATA platform is stabilized by $-BF_4$ counterions, while after deposition on a gold substrate the localization of the $-BF_4$ counterions remains unknown. We used 1,2,4–dichlorobenzene as solvent of TATA$-BF_4$ to induce the SAM formation on a warm (~50° C) Au substrate. In our STM experiments, we show how to detect and distinguish TATA platform with and without counterion on top. Finally, we observe a change of the counterion position on the SAM during the STM scanning, which appears due to an electric-field induced reduction of the electrostatic interaction in TATA$-BF_4$ on the surface. We applied DFT calculations to reveal the influence of the gold lattice and the electric field of the STM tip on the stability of the TATA$-BF_4$ precipitated on the surface.

TOC GRAPHICS

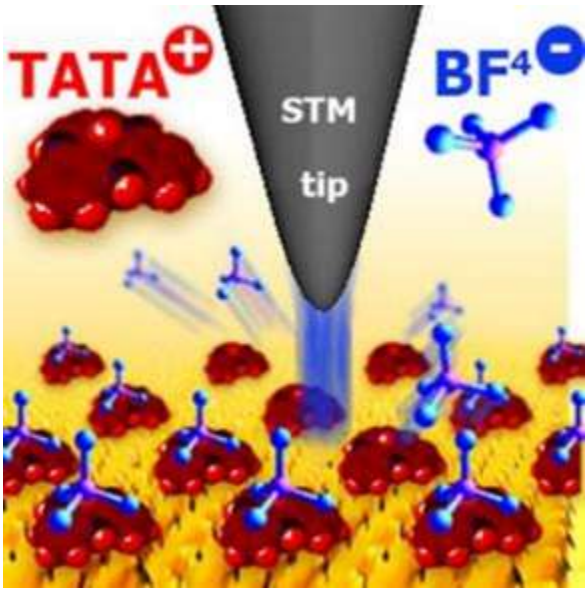

KEYWORDS triazatriangulenium, BF_4^-, cation, anion, STM, dissociation, gold, adhesion, bias dependence

INTRODUCTION

Controlled attachment of functional molecules to metal surfaces is of major interest in the field of molecular electronics. Self-organization approaches based on the competition between intermolecular interactions and molecular adsorption on surfaces, in organic molecules at the liquid/solid interface, is widely used for this purpose. It allows the formation of self-assembled monolayers (SAM) on different crystalline substrates.

Two approaches are widely used for SAM formation on Au(111). The first approach uses terminal alkanethiol molecules with a functional group on the second terminus. Due to the strong interaction between the alkyl chains, brush-like SAMs can be formed. Thiol end groups form strong covalent bonds with gold atoms.[1] The density of the resultant, strongly surface linked SAM is mainly determined by intermolecular interactions between the alkyl chains. As a result, the functional part on top of the SAM can be subject to steric repulsion.

The second approach is based on the use of platform-like molecules, which can carry on their top either a functional group or even molecules with specific functions.[2-5] A platform molecule should be an "in-between" molecule, with a structure able to generate derivatives, on which more complex architectures can be grown. One challenge is to elaborate such platforms on surfaces and ensure they can self-organize as physisorbed monolayers on various substrates, including Au(111).

One of these platforms is the cationic triazatriangulenium (TATA) with a large π-system and the tetrafluoroborate (BF_4^-) as its counterion in solution (**Figure 1).** Through chemical functionalization, the counterion can be replaced by a functional moiety, attached to the central carbon atom of TATA, which makes the functional unit free-standing in an almost perpendicular geometry with respect to the TATA-platform.[5-7] TATA derivatives belong to the most promising platforms for diverse functional molecules such as porphyrins,[8, 9] and azobenzenes .[6, 8, 10-17] However, these attached molecules require free space for their operation. Their lateral distance can be controlled either by the length of the nitrogen-bound side-chain R (Scheme 1, R= $-C_nH_{2n+1}$, n = 3-12)[15, 18] or by changing the applied potential during electrospray deposition of either the non-functionalized TATA−BF_4 or TATA–platform conjugates with e.g. an azobenzene moiety.[6, 12]

Despite the widespread application of TATA[5, 11, 12, 19] as platform, the role of the BF_4^- counterion for pattern formation in the SAM as well as its localization after self-organization on Au(111) is still unclear. With TATA−BF_4 deposited on a gold monocrystalline substrate, experiments using either X-ray photoelectron spectroscopy or electrochemical STM in $HClO_4$ electrolyte were unsuccessful to localize the BF_4^- counterions.[6, 12] It was concluded that about half of the TATA molecules are positively charged. If the applied electrochemical potential is decreased, discharging of the TATA monolayer occurred, leading to a transformation of the pre-adsorbed $\left(\sqrt{19} \times \sqrt{19}\right)R23.4°$ adlayer first into a ($7\sqrt{3} \times 7\sqrt{3}$) and then into a ($2\sqrt{3} \times 2\sqrt{3}$)R30° phase[12]. Earlier studies could not confirm the presence of BF_4^- either, and instead

argued that TATA molecules within the SAM were stabilized by electrons that come from the gold substrate.[15, 16]

Herein we will show that the self-assembly of TATA−BF_4 on the gold substrate leads mainly to decomposition of the molecule on TATA platform and BF_4.The TATA platform forms different molecular domains with two different orientations on the surface. By adjusting the STM tunneling parameters we could localize the presence of the BF_4^- counterions on some TATA platforms. Density functional Theory (DFT) calculations provide an explanation of the molecular adsorption process, as well as on the cohesion energy of the TATA−BF_4 molecule under the influence of the STM tip's electric field.

EXPERIMENTAL SECTION

Synthesis and purification of TATA−BF_4 with *n*-octyl side-chains (R = –$[CH_2]_7$–CH_3) (**Figure 1**) were performed according to ref. [17]. The purity of the synthesized TATA−BF_4 was unambiguously established by mass and NMR spectroscopy as well as by combustion analysis. (**Figure S1** in the Supplementary Information (SI)). The powder was stored at -18° C under N_2 atmosphere. All STM measurements were performed with freshly prepared solutions of TATA−BF_4 in the given solvent. We have used a lower concentration of molecules (1.3×10^{-7} mL^{-1}) compared to earlier work,[15, 16] to avoid the formation of a second molecular layer.

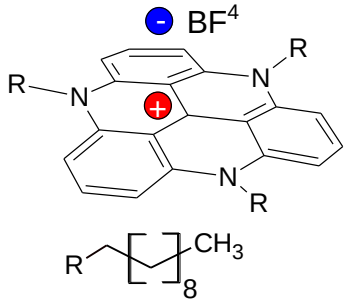

Figure 1 Chemical structure of the triazatriangulenium ($TATA^+$) with octyl (R) groups symmetrically attached to the three nitrogen atoms. The counterion to $TATA^+$ in solution is tetrafluoroborate (BF_4^-).

STM measurements. All SAMs were studied under ambient atmospheric conditions using a commercial STM equipped with a low-current head (Bruker, Nanoscope 3A). The calibration of the STM piezo ceramics is controlled regularly every month using a HOPG surface. The STM tip was prepared by mechanical cutting of a Pt/Ir (80:20) wire. For each monolayer, several STM images were recorded in constant current mode with the current setpoint ranging from 7 to 25 pA and tip bias from 0.1 to 1 V. Images were obtained for different samples using different tips to check the reproducibility and to ensure that the results are free from artefacts. All molecule-molecule distances given in the manuscript are averaged from different images and along

different crystallographic orientations to minimize errors caused by the thermal drift of the STM tip when working under ambient conditions.

The solutions of TATA molecules (1.3×10^{-7} mL^{-1}) in 1,2,4–dichlorobenzene was deposited on freshly annealed Au substrate. The substrate with the deposited solution was left on a heated plate (~50 °C) under ambient atmospheric pressure in the fume cabinet before the STM measurements. After about 1h of drying, a visual inspection of the substrate revealed complete evaporation of 1,2,4–dichlorobenzene, allowing STM measurements.

The gold surfaces are formed by thin films of evaporated gold on mica purchased from PHASIS (Switzerland). The substrate was annealed before deposition using a butane/propane torch so that clean Au(111) are prepared. The typical herringbone reconstruction of gold was considered as the evidence of surface purity.

Computational method

Density functional theory (DFT) calculations have been performed using the localized-orbital code Fireball[20]. In this approach, a self-consistent version of the Harris-Foulkes LDA functional[21,22] is used, instead of the traditional Kohn-Sham functional based on the electronic density. Hence, the potential is calculated by approximating the total charge by a superposition of spherical charges around each atom. The Fireball simulation package also uses a localized optimized minimal basis set[23], and the self-consistency is achieved over the occupation numbers through the Harris functional.[24] The optimized basis set is built using a linear combination of wavefunctions determined for the atom in its ground state and in a first excited state, in order to smoothen the decay of the radial part of the wavefunction and to optimize the overlaps between two neighboring atoms[23]. Besides, the LDA exchange-correlation energy is calculated using the efficient multi-center weighted exchange-correlation density approximation (McWEDA).[25,26] In the present work, the cut-off radii for the wavefunctions' radial part (for *s*, *sp* and *spd* basis sets) defining the optimized basis set are the following (in atomic units): r_s = 4.1 for H atom; r_s = 4.5, 4.2, 4.1 and 3.1, r_p = 4.5, 4.2, 4.1 and 3.9 for C, N, F and S atom respectively; r_s = 4.5 and 4.6, r_p = 4.9 and 5.2, r_d = 5.2 and 4.1 for the B and the Au atom, respectively. These optimized basis sets have been well-tested in previous works on molecular self-assembly on metallic surfaces.[27-28] we have determined the adsorption energy of the $TATA^+$ ion on the gold surface, with and without the counterion BF_4^-. The adsorption energy is defined in a standard manner as the difference between the total energy of the system and the energy of the isolated molecule and the isolated gold surface calculated independently. To this end, we have considered a 9×9–Au(111) slab composed of 5 layers in the *xy* plane, and we have set the $TATA^+$ or the TATA-BF_4 molecules on top. The structure has been optimized until the forces went below 0.1 $eVÅ^{-1}$, The interaction energy of the molecule with the surface has been calculated as a function of the molecule/surface distance. From the obtained equilibrium structure, we have determined the density of states (DOS). Also, to simulate the field effect of the STM tip, we have recalculated these adsorption energy curves with one extra electron in the system, following previous work on hydrogen porphyrin tautomerization.[29]

EXPERIMENTAL OBSERVATIONS

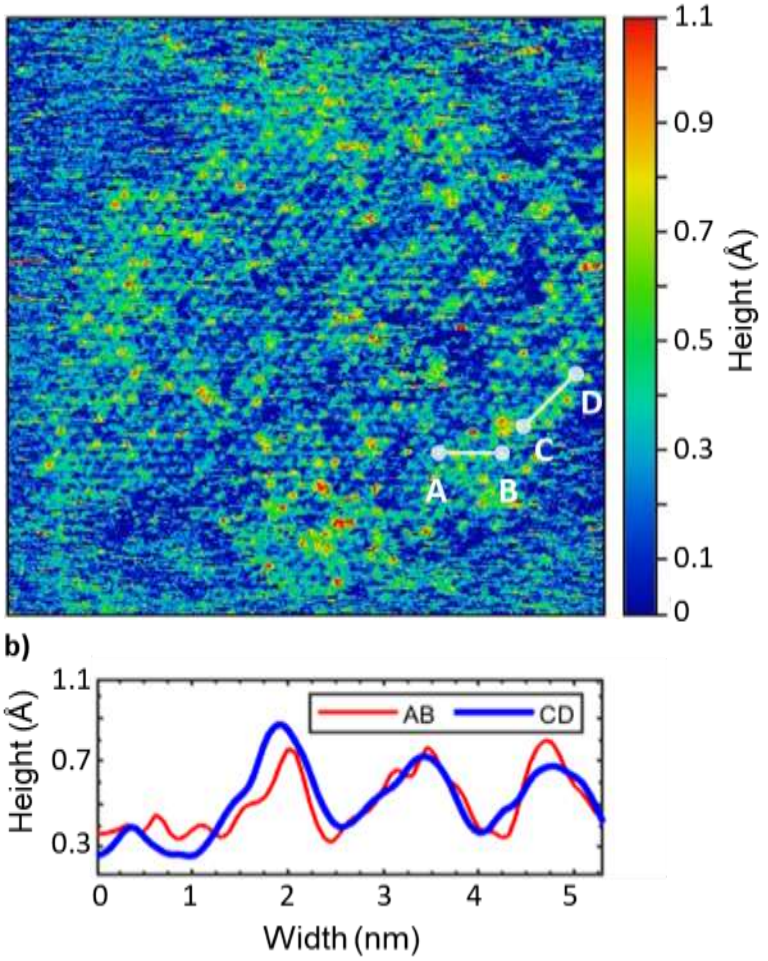

Figure 2 a) STM image 56×56 nm^2 of SAM of TATA–BF_4 molecules deposited on Au(111). The corresponding STM parameters are U_t = 0.3 V, I_t = 15 pA. **b**) Cross sections along corresponding directions in **a**) represent the relative height profiles of some red protrusions. The color-code is the same for all images in this article.

STM contrast variation of SAM

The initial STM studies of the Au(111) surface done directly after evaporation of 1,2,4–dichlorobenzene do not reveal the formation of a SAM. The first indication of the assembly is observed only after the samples were kept on the heated plate at 50 °C for an additional 2 h after the solvent evaporation was complete. Hence, we can deduce that the diffusion process is essential for the molecule to overcome the interaction energy with the Au(111) surface. Namely, the intramolecular interactions are weaker than the molecule-surface interaction.

Figure 2 represents a small area of the Au(111) surface with a clear indication of a SAM. The STM contrast of the SAM is formed by a periodic pattern of quasi-round shaped spots (green), **Figure 2a**). The measured average distance between neighboring spots is ~ 13.8 Å (**Figure 2b**). We associate each spot with one single TATA molecule, as we will explain further below. The color profile in **Figure 2a** allows estimating that almost 20% of the spots appear as red protrusions, corresponding to a 0.4 Å bigger relative height than their neighbors (**Figure 2b**).

Continuous STM scanning of the surface area in **Figure 2** using the same tunneling parameters (U_t = 0.3 V, I_t = 15 pA) does not change the contrast of the pattern, revealing the stability of the formed monolayer and that thermal motion of the TATA platforms can be neglected. However, during scanning local distortions in the vicinity of the red protrusions became apparent. Even

though these protrusions have a similar height profile and separation distance (**Figure 2b**), their position within the SAM changed while scanning.

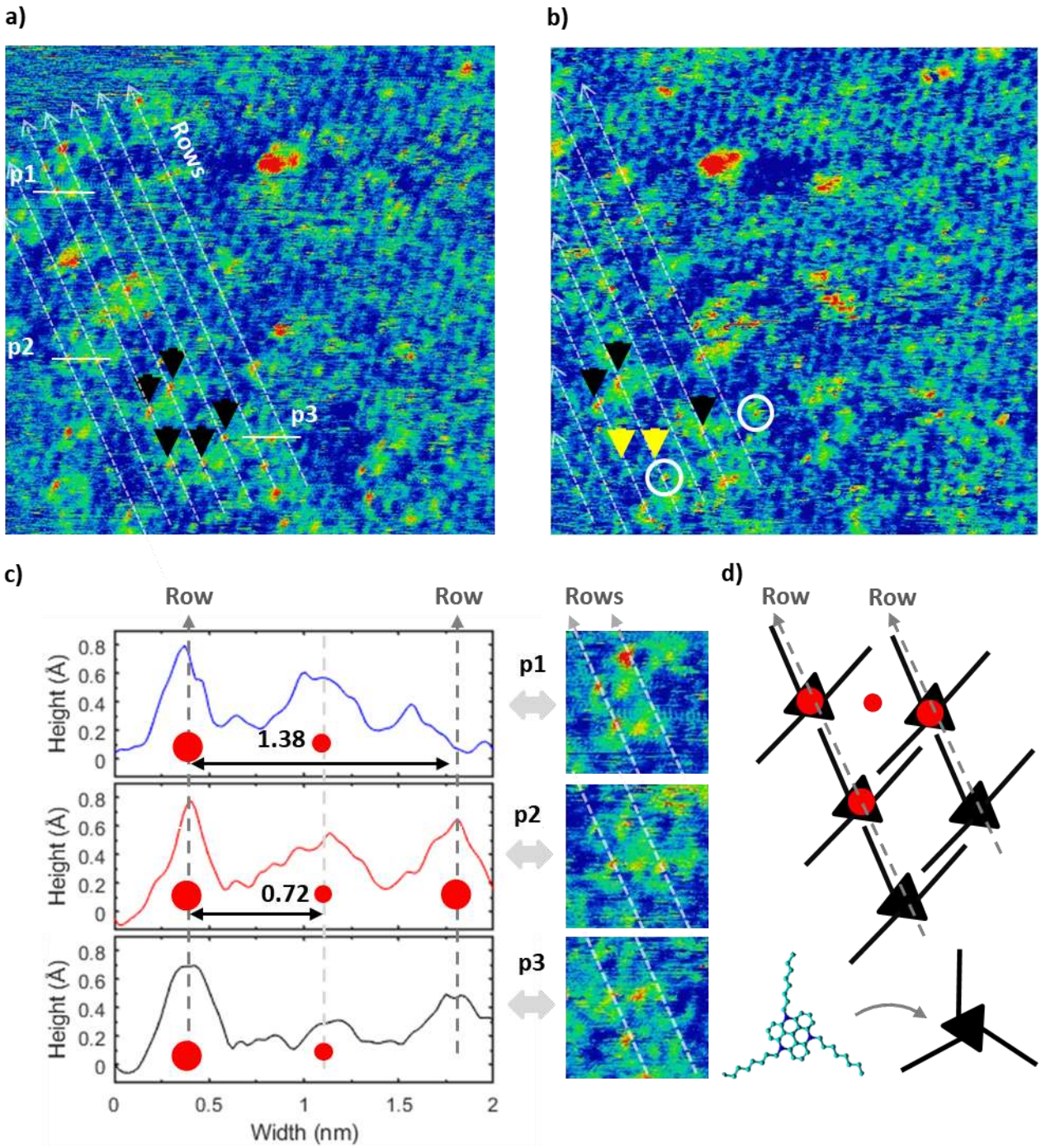

Figure 3. Two consecutively obtained STM images of the same area (23 × 23 nm^2) recorded under the same tunneling conditions (U_t = 0.3 V, I_t = 15 pA). The large red object in the top-center is used as the reference object. Black arrows point on some protrusions that did not change their positions while the yellow arrows on **b)** point on the places where protrusions disappeared, compared with **a)**. White circles in **b)** point on positions where the red spots

appeared compared to **a)**. The color-code is the same as for **Figure 2**. The cross-sections p1-p3 in **c)** represent the relative height of red protrusions when they are located on top of the row or in between rows. The small STM images (4.2×4.2 nm^2) on the right section of **c)** were cut from **a)** where cross-sections were measured. **d)** - Possible locations of the red protrusions with presented according to proposed molecules packing (see below).

Figure 3a shows an enlarged area of **Figure 2** with the black arrows pointing on several randomly selected red protrusions. After recording the next image (**Figure 3b**), using the same tunneling parameters (U_t = 0.3 V, I_t = 15 pA), some of these protrusions disappeared (yellow arrows in **Figure 3b**), while others remain at their initial positions (black arrows in **Figure 3b**). The periodic arrangement of all maxima remains intact. Furthermore we found, that the majority of the red protrusions were located along particular rows (white lines in **Figure 3a,b**). According to the cross-sections p1 to p3, shown in **Figure 3c**, the red protrusion in neighboring rows are separated by ~13.8 Å from each other. However, in some cases, the protrusions can be found exactly in between the rows (right section of **Figure 3c**) with the separation distance ~0.72 Å. Their STM contrast is different to the red protrusions detected within a row and the relative height is also smaller than 0.4 Å, measure for red protrusions along the rows (right section of **Figure 3c**). On the basis of the earlier observations in ref. [6,12] we assumed that the rows can be associated with the position of the TATA-BF_4 molecules (Figure 3d), which might explain the difference in the STM contrast and the relative height of these protrusions. Therefore, to further reveal the nature of the rows where the majority of the red protrusions are localized, a set of STM images was recorded for the same surface area as in **Figure 3** under higher tunneling bias and current. A transition image **Figure S3** showig the left part of **Figure 2,** but recorded at a higher bias (0.45 V)**.** Instead of protrusions an array of separated almost circular objects with a black spot in the center is observed. A further increase of the tunneling parameters (0.6 V, 20 pA) led to the appearance of triangular-shaped objects without evident STM contrast difference between each other and without protrusions (**Figure 4**). We associate each triangle with the position of an aromatic core of a single TATA-BF_4 molecule based on comparison with the calculated shape of the highest occupied molecular orbital (HOMO) of TATA (see Theoretical modeling). In ambient STM it is not possible to image the alkyl side chains. Therefore we cannot determine the precise relative alignment of the chains and the orientation of the TATA cores with respect to each other. However, combining the information from the modeling and from the periodicity of the STM images we conclude that the position and orientation of the rows, where the red protrusions are located in Figure 3, correspond to rows of TATA-BF_4 molecules (Figure 4).

The arbitrarily located empty areas without triangles can be assigned to vacancies in the SAM (blue areas marked by white arrows in **Figure 4a**. Continuous scanning with the same tunneling parameters (0.6 V, 20 pA) of the same area reveals that the vacancies can change position. Furthermore, the shape of the assembled domain (**Figure 4 ab**) may vary and new domains may form (left parts in **Figure 4b)**. Inspection of the domains reveals two orientations

of molecular rows rotated by 34 ± 2 ° with respect to each other, revealing a lower symmetry than expected for the rotation on an Au(111) facet with six-fold symmetry.

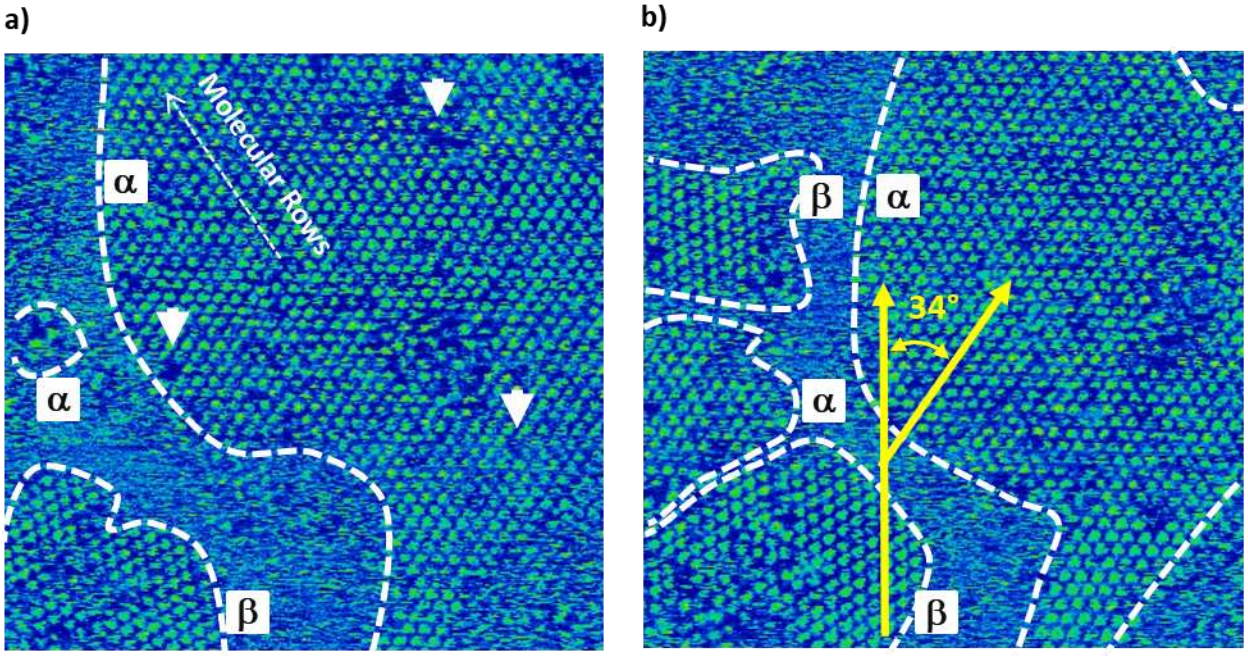

Figure 4. Two consecutively recorded STM images (38.5×38.5 nm^2) of a SAM of TATA−BF_4 molecules on Au(111). Two types of hexagonally ordered domains, α and β, surrounded by disordered regions are formed. The angle between the molecular rows of the two domains is ~34 ± 2°. The STM parameters are U_t = 0.6 V, I_t = 20 pA. The white arrows on **a**) points on vacancies.

Therefore, we argue about the presence of two types of molecular packing, which leads to the formation of domains, named α and β. Additional analysis of the domains using two dimensional fast Fourier transformation (2d-FFT) also revealed a difference between the domains. (**Figure S4**).The α domain has a slightly distorted hexagonal arrangement with lattice constants spacing a = 13.8 ± 0.6 Å and b = 15.0 ± 0.4 Å. The β domain has hexagonal packing with molecules spacing of 13.8 ± 0.6 Å. The orientation of the triangles (molecules) within a row of each domain is the same but different in both domains. **Figure 4cd** shows two possible arrangements of the TATA molecules and their side chains which are compatible with the observed periodic patterns. Further investigations are necessary to confirm the orientations of the alkyl chains, though, see also discussion about **Figure S5.**

Theoretical modeling of TATA−BF4 on Au(111). The electronic and structural properties of the TATA−BF_4 molecule have been investigated using DFT. We have first optimized the isolated molecule, and then the molecule adsorbed on a 3 atoms thick gold surface until the forces went below 0.01 eV/Å **(Figure 5a)**. From these optimized configurations, we have

determined the cohesion energy between the $TATA^+$ cation and the BF_4^- anion. This energy is decisive to understand the dissociation mechanism of the complex on the Au surface. The evolution of the cohesion energy for both the molecule and the molecule adsorbed on Au(111) as a function of the distance between the $TATA^+$ and BF_4^- (measured between the topmost atom of $TATA^+$ and the bottommost atom of BF_4^-) is represented in **Figure 5b**. As a result, we obtain a cohesion energy of about 1.8 eV for the isolated complex and 3.0 eV for the molecule adsorbed on Au(111). Therefore, the TATA−BF_4 molecule is stabilized by adsorption on the gold surface. We note that, since DFT is a ground-state theory and we consider a simplified model, we do not expect the absolute energy values to be quantitatively in agreement with the experiment. However, relative changes between the different systems are well reproduced by the theory

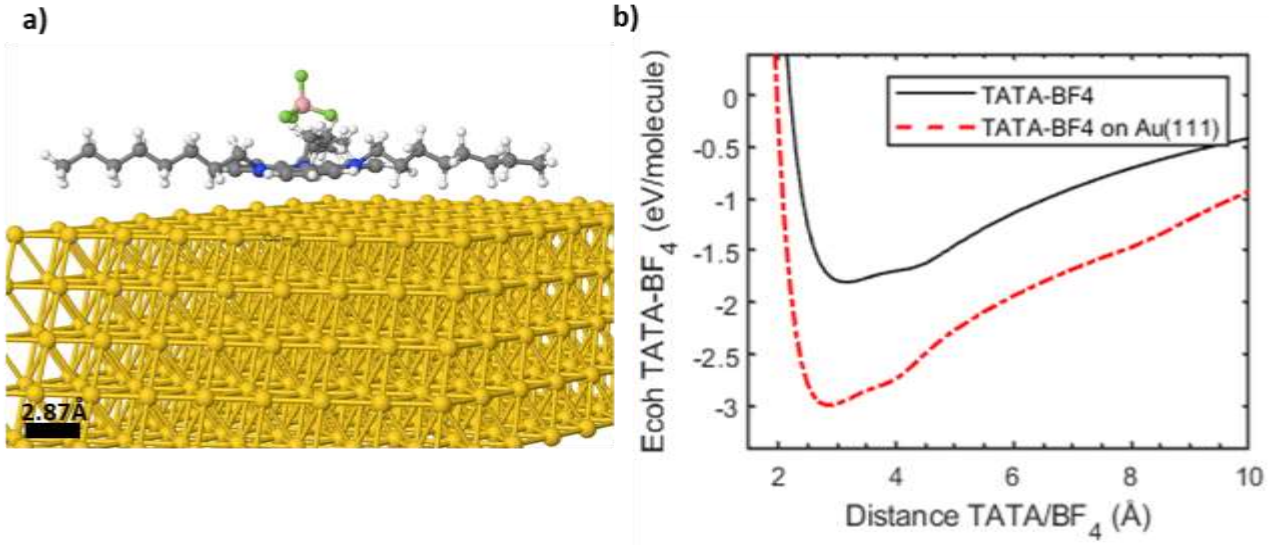

Figure 5. a) DFT-optimized configuration of the TATA−BF_4 molecule adsorbed on the Au(111) surface. **b)** Evolution of the cohesion energy for the isolated (solid line) and adsorbed on Au(111) (dash-dotted line) TATA−BF_4, as a function of the distance between BF_4^- and $TATA^+$.

Furthermore, we have determined the DOS of the TATA platform (without BF_4) adsorbed on Au(111). We found a HOMO level located at around 1.6 eV below the Fermi level. Consequently, we have calculated the corresponding isoelectronic DOS for a charge density of 0.001 e/$Å^3$ of this level, which is the one observed experimentally in the STM images. Both results are represented in **Figure 6**. We can observe that the molecular orbital is centered on the aromatic core of the TATA molecule, with very little contribution on the alkyl chains.

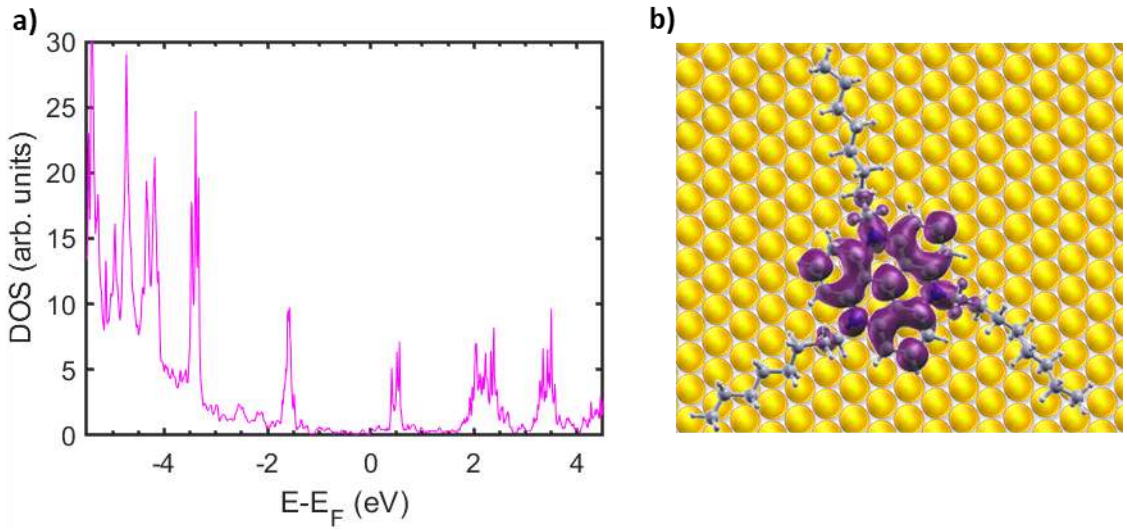

Figure 6. a) DFT calculated DOS of $TATA^+$ platform adsorbed on Au(111). **b)** Corresponding isoelectronic DOS at 0.001 e/Å^3. The $TATA^+$ HOMO level exhibits the triangular symmetry observed in the STM images.

DISCUSSION

The observation of a single hexagonal type of molecular packing (domain α, **Figure 2**) is in agreement with the observations of Lemke and coworkers when electrochemical STM was used,[12] suggesting that only one packing structure of TATA−BF_4 with a minimum of the free energy can exist on Au(111). However, the next few scans of the same area (**Figure 3a**) revealed the presence of a growing domain β with different orientation and intermolecular separation. This observation proofs that at least two energetically favorable packing structures can coexist. However, the exact mechanism of formation of this β domain in **Figure 4a** could not be traced. It might have formed already during the process of the solvent evaporation or only under the action of the STM tip. Nevertheless, both domain types can be formed and increase in size on Au(111) lattice during the STM operation (**Figure 4a,b**). A similar effect of STM tip-induced assembling was observed for an aryltriazole salt, where different packings were observed after repeated scanning and were attributed to the interaction with the tip.[30] It is noteworthy that in our study the STM interaction does not induce a domain reordering or change of the local packing density, in contrast to observations made with electrochemical STM.[12] Instead, the electric field might excite vibrations of the molecules within a SAM, allowing their soft motion, which explains the observed relocations of the positions of molecular vacancies within a SAM (**Figure 4**). Therefore, we argue that the interaction of the tip with the molecule can lead to a reorientation of the peripheral alkyl chains of the molecules on the surface.[12] Such reorientation may foster the motion of the entire molecule on the surface, supporting the formation of two domains α and β, where the peripheral alkyl chains have to occupy slightly different positions on the surface, as shown in the model of molecular packing **Figure 3d**. Note, that in the model we used a hypothesized orientation of the alkyl chains, since their exact position on the surface was

not possible to observe experimentally, although different tunneling conditions were tested. The structure and orientations of the aromatic cores of the platforms in **Figure 3d,S5** are proposed according to the STM contrast of the SAM observed under $U_t = 0.6$ V in **Figure 4**. Under these conditions, the STM contrast of the molecule has a triangular shape, which is consistent with the DFT modeling results of the HOMO of the TATA platform without BF_4 (**Figure 6b**). This allows us to conclude that the triangular-shaped spots correspond to TATA platforms that lost their counterions. This hypothesis is also supported by earlier X-ray photoelectron spectroscopy and electrochemical STM in $HClO_4$ electrolyte, where no signatures of BF_4^- for precipitated TATA−BF_4 molecules on Au were observed.[6, 12]

To understand the high abundance of TATA without counterions, we have explored theoretically the influence of the electric field of the STM tip on the TATA−BF_4 molecular dissociation. Indeed, it is well known that during the acquisition of an STM image, the electric field of the tip can induce several processes in the observed system. For example, a common effect is the shift of the molecular levels in systems modeled by a double barrier tunneling due to the weak interaction with the surface. Hence according to the bias polarity, either the HOMO or the LUMO level can be found pinned at the Fermi level,[31] allowing removing or adding one electron to the system, respectively. Furthermore, it has also been shown that the electric field of the STM tip can induce a tautomerization process in a hydrogen phthalocyanine molecule adsorbed on graphene. [29] Here in the same manner, since the TATA molecule interacts weakly with the Au surface, the double tunnel barrier model applies as well and we can expect the same effects on shifting the levels and adding or removing charges to the molecule. To simulate the influence of the electric field, we have recalculated the cohesion energy of the TATA−BF_4 complex isolated and adsorbed on a Au cluster with an electron added to the system.

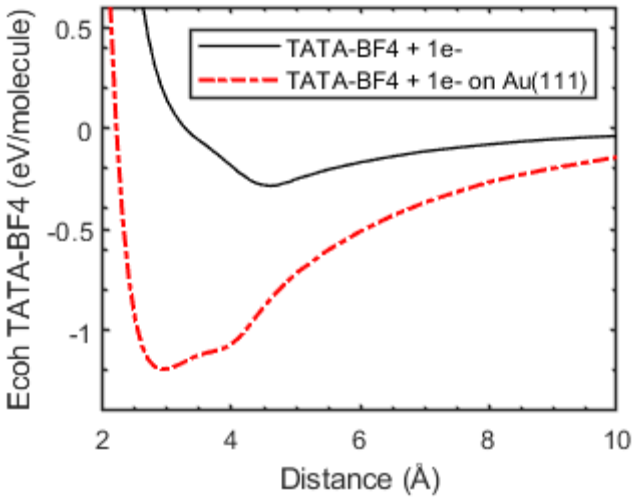

Figure 7. Evolution of the cohesion energy of TATA−BF_4 (with one extra electron to simulate the effect of the electric field of the STM tip) for the isolated and adsorbed case, as a function of the TATA−BF_4 distance.

As a result, we can observe a drastic reduction of the corresponding cohesion energy when adsorbed on the surface (**Figure 7**). The cohesion energy of the isolated/adsorbed molecule ranges from 1.8 to about 0.3 eV/ 3.0 to 1.2 eV. Consequently, we can deduce that the dissociation mechanism of the TATA−BF_4, even though stabilized by the gold surface, is favored by the electric field of the STM tip. These findings might explain the dissociation process of TATA−BF_4 on the gold surface. This shows that the red protrusions (**Figure 2,3)** that were observed under the lowest tunneling bias (0.3 V) with non-uniform 2D pattern contrast of the TATA platforms can be attributed to BF_4^- anions. They are localized in the row of the TATA platforms (**Figure 3**) with a separation equal to the one between TATA platforms. Consequently, they can be localized on the top of some TATA platforms. Obviously, these protrusions might be related to the formation of the second adlayer of the TATA platform, monitored earlier.[6] However, the relative height differences ~0.4 ± 0.1 Å measured for these red protrusions along the molecular row (**Figure 2b**) was found to be much smaller than the 4 Å reported as the thickness of the second adlayer [15]. In this regard, the observations of the position change of some redprotrusions in **Figure 3** can be explained by the motion of BF_4 anions on the SAM, induced by the electric field of the STM tip. Such a motion explains the observed modification and distortions in the STM images in **Figures 2 and 3**. Moreover, each position of protrusions on the STM images is surrounded by a halo (green color around the protrusions on **Figure 3 a, b**), which also disappears if the relevant protrusion changes the position. We associate this variation of the halo with the variation of the local DOS of the corresponding TATA within the SAM. From these observations, we argue that these protrusions are BF_4^-, present on about 15 to 20% (calculated from **Figure 2a**) of all TATA platforms within a SAM of the α domain (**Figure 2**), while the rest of the platforms are stabilized, presumably, by electrons coming from the lattice, as proposed in earlier studies.[15, 16] The "invisible" rest of the BF_4 anions can still be present on the surface but might be so mobile that they are pushed out from the scan area, unless they fall into a local "trap". Such trap can be the area in between the TATA platforms that restrict BF_4^- motion during the STM scanning (cross-sections p1-p3 in **Figure 3c**). However, the probability that these traps can catch BF4 is even less than being catched by TATA platforms, comparing the amount of red protrusions on the rows and in between them (Figure 3a). Thus, the observed arbitrary dispersion of BF_4^- within a TATA SAM and the dissociation of the initial complexes can be described as a random process.

CONCLUSIONS

To summarize, STM measurements TATA−BF_4 deposited on an Au(111) surface demonstrate that these molecules self-assemble into a stable monolayer at room temperature. A diffusion process is activated at around 50 °C and the molecules form a SAM, with two distinct domains corresponding to two types of molecular packings. The domain size with the intrinsic packing structure can increase under the influence of the electric field in the tunneling gap of the STM.

Interaction of the TATA−BF_4 molecule with the gold lattice lowers the strength of the ionic bond between the $TATA^+$ cores and the BF_4 counterions. DFT calculations support the suppression of the TATA−BF_4 bonding upon adsorption on Au(111) and reveal the influence of the electric field of the STM tip in the full dissociation of the complex. Therefore, STM allows identifying single TATA molecules, but we also show that a small number of these molecule still accommodate the BF_4 counterion on them. It can be detected by STM exclusively when using small tunnel voltages.

Thus, the interaction of the Au(111) surface with the molecules that have ionic bonds can lead to dissociation of the last. This effect can be reinforced by the electric field, which requires the use of delicate STM tunneling parameters to visualize both the parent ion and its counterion.

ASSOCIATED CONTENT

Supporting Information contains; additional STM images with highlighted results of FFT analysis of α and β domains; STM images recorded under the different tunneling parameters; proposed model of molecular packing with possible positions of BF4 counterions on TATA platforms. The following files are available free of charge.

AUTHOR INFORMATION

Corresponding Author
*** E-mail: sergii.snegir@uni-konstanz.de**
Notes
The authors declare no competing financial interests.

ACKNOWLEDGMENT

The authors appreciate the financial support of: the Deutsche Forschungsgemeinschaft through the projects SFB767, Plasmochrome and the Ministry of foreign affairs of France for granting a personal scholarship for Sergii Snegir.

REFERENCES

1. J. C. Love, L. A. Estroff, J. K. Kriebel, R. G. Nuzzo and G. M. Whitesides, *Chem. Rev.*, 2005, **105**, 1103-1169.
2. R. Otero, J. Maria Gallego, A. L. Vazquez de Parga, N. Martin and R. Miranda, *Adv. Mater.*, 2011, **23**, 5148-5176.
3. S. Mohnani and D. Bonifazi, *Coord. Chem. Rev.*, 2010, **254**, 2342-2362.
4. C. M. Drain, A. Varotto and I. Radivojevic, *Chem. Rev.*, 2009, **109**, 1630-1658.
5. T. Jasper-Tönnies, A. Garcia-Lekue, T. Frederiksen, S. Ulrich, R. Herges and R. Berndt, *J. Phys.: Condens. Matter*, 2019, **31**, 18LT01.
6. U. Jung, S. Kuhn, U. Cornelissen, F. Tuczek, T. Strunskus, V. Zaporojtchenko, J. Kubitschke, R. Herges and O. Magnussen, *Langmuir*, 2011, **27**, 5899-5908.
7. N. R. Krekiehn, M. Mueller, U. Jung, S. Ulrich, R. Herges and O. M. Magnussen, *Langmuir*, 2015, **31**, 8362-8370.
8. F. L. Otte, S. Lemke, C. Schuett, N. R. Krekiehn, U. Jung, O. M. Magnussen and R. Herges, *J. Am. Chem. Soc.*, 2014, **136**, 11248-11251.
9. N. Hauptmann, L. Gross, K. Buchmann, K. Scheil, C. Schutt, F. L. Otte, R. Herges, C. Herrmann and R. Berndt, *New J. Phys.,* 2015, **17**, 013012- 013020.
10. M. Hammerich and R. Herges, *J. Org. Chem.*, 2015, **80**, 11233-11236.
11. S. Ulrich, U. Jung, T. Strunskus, C. Schuett, A. Bloedorn, S. Lemke, E. Ludwig, L. Kipp, F. Faupel, O. Magnussen and R. Herges, *Phys. Chem. Chem. Phys.,* 2015, **17**, 17053-17062.
12. S. Lemke, C.-H. Chang, U. Jung and O. M. Magnussen, *Langmuir*, 2015, **31**, 3115-3124.
13. U. Jung, C. Schuett, O. Filinova, J. Kubitschke, R. Herges and O. Magnussen, *J. Phys. Chem. C*, 2012, **116**, 25943-25948.
14. S. Kuhn, U. Jung, S. Ulrich, R. Herges and O. Magnussen, *Chem. Commun.*, 2011, **47**, 8880-8882.
15. S. Kuhn, B. Baisch, U. Jung, T. Johannsen, J. Kubitschke, R. Herges and O. Magnussen, *Phys. Chem. Chem. Phys.,* 2010, **12**, 4481-4487.
16. B. Baisch, D. Raffa, U. Jung, O. M. Magnussen, C. Nicolas, J. Lacour, J. Kubitschke and R. Herges, *J. Am. Chem. Soc.,* 2009, **131**, 442-443.
17. B.W. Laursen, F.C. Krebs, *Chem. Eur. J.,* 2001, **7**, 1773-1783.
18. S. Lemke, S. Ulrich, F. Claussen, A. Bloedorn, U. Jung, R. Herges and O. M. Magnussen, *Surface Science*, 2015, **632**, 71-76.
19. J. Kubitschke, C. Näther and R. Herges, *Eur. J. Org. Chem.*, 2010, **2010**, 5041-5055.
20. J. P. Lewis, P. Jelínek, J. Ortega, A. A. Demkov, D. G. Trabada, B. Haycock, H. Wang, G. Adams, J. K. Tomfohr, E. Abad, H. Wang and D. A. Drabold, *Phys. Status Solidi B*, 2011, **248**, 1989-2007.
21. J. Harris, *Phys. Rev. B*., 1985, **31**, 1770–9.
22. W.M.C. Foulkes, R. Haydock, *Phys. Rev. B.,* 1989, **39**, 12520–36.
23. M. A. Basanta, Y. J. Dappe, P. Jelínek and J. Ortega, *Comput. Mater. Sci.*, 2007, **39**, 759-766.
24. A.A. Demkov,J. Ortega,O.F. Sankey, M.P. Grumbach, *Phys. Rev. B.* 1995, **52**,1618–30.
25. P. Jelı´nek, H. Wang, J.P Lewis, O.F. Sankey, J. Ortega, *Phys. Rev. B.* 2005, **71**, 2351011–9.
26. O.F. Sankey, D.J. Niklewski, *Phys. Rev. B.* 1989, **40**, 3979–95.

27. S. Snegir, Y. J. Dappe, O. L. Kapitanchuk, D. Coursault and E. Lacaze, *Phys. Chem. Chem. Phys.*, 2020, **22**, 7259-7267.
28. P. Sleczkowski, Y. J. Dappe, B. Croset, Y. Shimizu, D. Tanaka, R. Minobe, K. Uchida and E. Lacaze, *J. Phys. Chem. C*, 2016, **120**, 22388-22397.
29. R. Harsh, F. Joucken, C. Chacon, V. Repain, Y. Girard, A. Bellec, S. Rousset, R. Sporken, A. Smogunov, Y. J. Dappe and J. Lagoute, *J. Phys. Chem. Lett.*, 2019, **10**, 6897-6903.
30. B. E. Hirsch, K. P. McDonald, B. Qiao, A. H. Flood and S. L. Tait, *ACS Nano*, 2014, **8**, 10858-10869.
31. V. D. Pham, S. Ghosh, F. Joucken, M. Pelaez-Fernandez, V. Repain, C. Chacon, A. Bellec, Y. Girard, R. Sporken, S. Rousset, Y. Dappe, J. S. Narasimhan and J. Lagoute, *NPJ 2D Mater. Appl.*, 2019, **3**, UNSP 5.
32. L.A.Rochford, I.Hancox, T.S.Jones *Surf. Sci.*, 2014, **628**, 62-65.